LCLS-II Undulator Beam Pipe Corrector Calibration

Zachary Wolf, Yurii Levashov
Stanford Linear Accelerator Center

May 4, 2020

Abstract

Background magnetic fields in the undulator tunnel are different than in the measurement laboratory. The undulators are tuned to remove the effect of the background field in the laboratory. When the undulators are moved to the tunnel, the different background field affects the undulator perameters using up or exceeding the tolerance budget. The difference between the background field in the tunnel and the laboratory is compensated by corrector windings on the beam pipe. This note analyzes the problem of the background field difference and it presents measurement results giving a calibration of the beam pipe corrector windings.

1 Introduction[1]

The beam trajectories in the LCLS-II undulators are tuned in the laboratory to be straight at all gaps. When the undulator is placed in the tunnel in a different background magnetic field, the trajectories become curved, reducing the undulator performance. Correction coils have been build into the beam pipe to mitigate this problem. The current required in the correction coils depends on the magnitude and direction of the difference in the background magnetic field between the tunnel and the lab, and the current also depends on the undulator gap. The magnetic field in the tunnel has been mapped, so the difference in background fields is known. In the lab this difference is simulated by a large Helmholtz coil. The effect of the field difference must be determined as a function of undulator gap, and the current in the trim windings to correct the difference must be determined. We do this for one representative undulator of each type, and assume all undulators of each type behave similarly. Determining the behavior of the undulators in an external field and performing the calibration of the beam pipe correctors are the subjects of this note.

The measurements took place in January and February, 2020. The SXR undulator used for the test was SXU-021. The HXR undulator used for the test was HXU-031.

2 Undulator Tuning Requirements

In order to discuss the relevance of the effect of changes in the background magnetic fields, we must know how the field difference affects the undulator parameters relative to the

[1]Work supported in part by the DOE Contract DE-AC02-76SF00515. This work was performed in support of the LCLS project at SLAC.

tolerances on the parameters. The LCLS-II undulator tolerances come from an undulator Physics Requirements Document[2]. The list of tuning requirements relevant to this note are briefly summarized below.

2.1 SXR Requirements

1. The K value must be known to $\pm 3 \times 10^{-4}$ at all gap settings.
2. The phase shake in each undulator must be less than 5 degrees rms.
3. The total phase advance in the 4.40000 meter long cell must be known to ± 10 degrees.
4. The first field integral of B_x and B_y must be within $\pm 40 \times 10^{-6}$ Tm of zero. The second field integral of B_x and B_y must within $\pm 150 \times 10^{-6}$ Tm^2 of zero.

2.2 HXR Requirements

1. The K value must be known to $\pm 2.3 \times 10^{-4}$ at all gap settings.
2. The phase shake in each undulator must be less than 4 degrees rms.
3. The total phase advance in the 4.01267 meter long cell must be known to ± 5 degrees.
4. The first field integral of B_x and B_y must be within $\pm 40 \times 10^{-6}$ Tm of zero. The second field integral of B_x and B_y must be within $\pm 150 \times 10^{-6}$ Tm^2 of zero.

3 Effect Of The Background Field Difference

As noted in the introduction, the beam trajectories in the undulators are tuned to be straight (within tolerance). This is done in the presence of a background magnetic field in the laboratory. When the undulators are moved to the tunnel, the background magnetic field is different. The extra field causes the beam to follow a circular path, approximated as parabolic, through the undulator. A beam position monitor at the end of the undulator senses when the beam is off the axis, and a feedback control system uses corrector magnets at the ends of the undulator to move the beam back to the undulator axis at the BPM position. So the path of the beam through the undulator is parabolic and goes to zero at each end of the undulator. In this section we estimate the consequences of this curved trajectory.

Consider an HXR undulator with an additional constant field $\overrightarrow{b}_0$ in the x-direction on the beam axis. The change in beam trajectory is given by

$$\frac{d}{dt}\left(\gamma m \overrightarrow{v}\right) = q \overrightarrow{v} \times \overrightarrow{b}_0 \tag{1}$$

The additional contribution to the y-trajectory is given by

$$y'' = \frac{q}{\gamma m v_z} b_0 \tag{2}$$

[2] H. D. Nuhn et al., "Undulator System Requirements", LCLS-II Physics Requirements Document LCLSII-3.2-PR-0038-R3.

where the prime indicates d/dz. For small changes to the trajectory, we treat v_z as constant. We also treat γ as constant. In this case

$$y = \frac{1}{2}\frac{q}{\gamma m v_z} b_0 z^2 + Az + B \tag{3}$$

for constants A and B. We take $z = 0$ as the center of the undulator. We constrain the beam so that $y = 0$ at $z = -L/2$ and $z = +L/2$, where L is the undulator length, which we approximate to be the same as the cell length. With these constraints, we find

$$y = \frac{1}{2}\frac{e}{\gamma m v_z} b_0 \left[\left(\frac{L}{2}\right)^2 - z^2 \right] \tag{4}$$

where we made the substitution $q = -e$, where e is the magnitude of the electron charge. The sagitta is the value of y at $z = 0$.

$$\text{Sagitta} = \frac{1}{2}\frac{e}{\gamma m v_z} b_0 \left(\frac{L}{2}\right)^2 \tag{5}$$

The trajectory slope is given by

$$y' = -\frac{e}{\gamma m v_z} b_0 z \tag{6}$$

The extra path length is given by

$$\begin{aligned} \delta L &= \int_{-L/2}^{L/2} \sqrt{1 + y'^2}\, dz - L & (7) \\ &\simeq \int_{-L/2}^{L/2} \frac{1}{2} y'^2 dz & (8) \end{aligned}$$

Performing the integral gives

$$\delta L = \left(\frac{e}{\gamma m v_z} b_0\right)^2 \frac{1}{3} \left(\frac{L}{2}\right)^3 \tag{9}$$

The slippage through the undulator from the vertical trajectory is given by

$$S(z) = \int_{-L/2}^{z} (\frac{1}{2}\frac{1}{\gamma^2} + \frac{1}{2} y'^2) dz \tag{10}$$

For a sinusoidal field in the undulator of the form

$$B_x = B_0 \sin(\frac{2\pi z}{\lambda_u}) \tag{11}$$

the sinusoidal trajectory slope is given by

$$y' = -\frac{K}{\gamma} \cos(\frac{2\pi z}{\lambda_u}) \tag{12}$$

where

$$K = \frac{e}{mv_z}(\frac{\lambda_u}{2\pi})B_0 \tag{13}$$

Combining the sinusoidal trajectory with the parabolic trajectory from the difference in background magnetic field, we get a trajectory slope

$$y' = -\frac{K}{\gamma}\cos(\frac{2\pi z}{\lambda_u}) - \frac{e}{\gamma m v_z}b_0 z \tag{14}$$

The slippage over the undulator length is given by

$$\begin{aligned} S &= \int_{-L/2}^{L/2}\left(\frac{1}{2}\frac{1}{\gamma^2} + \frac{1}{2}\left[-\frac{K}{\gamma}\cos(\frac{2\pi z}{\lambda_u}) - \frac{e}{\gamma m v_z}b_0 z\right]^2\right)dz & (15)\\ &= \frac{1}{2\gamma^2}\left(1+\frac{1}{2}K^2\right)L + \left(\frac{e}{\gamma m v_z}b_0\right)^2\frac{1}{3}\left(\frac{L}{2}\right)^3 & (16)\end{aligned}$$

The first term is the slippage through the undulator without the added trajectory curvature, and the second term is the additional slippage from the parabolic trajectory, which is equal to the extra path length of the trajectory given in equation 9.

In order to approximate the change in the K value from the added curvature, we rewrite the slippage as

$$S = \frac{1}{2\gamma^2}\left(1+\frac{1}{2}K^2 + \frac{1}{2}\left(\frac{e}{mv_z}b_0\right)^2\frac{1}{6}L^2\right)L \tag{17}$$

We define the new K value, K_b, from the slippage using the following formula similar to the $b_0 = 0$ case

$$S = \frac{1}{2\gamma^2}\left(1+\frac{1}{2}K_b^2\right)L \tag{18}$$

This gives

$$K_b^2 = (K+\delta K)^2 = K^2 + \left(\frac{e}{mv_z}b_0\right)^2\frac{1}{6}L^2 \tag{19}$$

The change in K is

$$\delta K \simeq \frac{1}{2K}\left(\frac{e}{mv_z}b_0\right)^2\frac{1}{6}L^2 \tag{20}$$

The relative change in K is

$$\frac{\delta K}{K} = \frac{1}{2K^2}\left(\frac{e}{mv_z}b_0\right)^2\frac{1}{6}L^2 \tag{21}$$

This is an approximation because in practice the K value is calculated from a linear fit to the slippage vs z curve, and here we are only using the end points, making it more sensitive to the shape of the curve. The approximation, however, is useful for determining if the extra trajectory curvature causes changes to K near the tolerance. We see that the relative change in K due to the trajectory curvature becomes large at small K. If we assume $b_0 = 0.2$ G over the length between BPMs of $L = 4.01267$ m, we get the relative change in K as a function of K shown in figure 1. The range in K corresponds to the 7.2 to 20

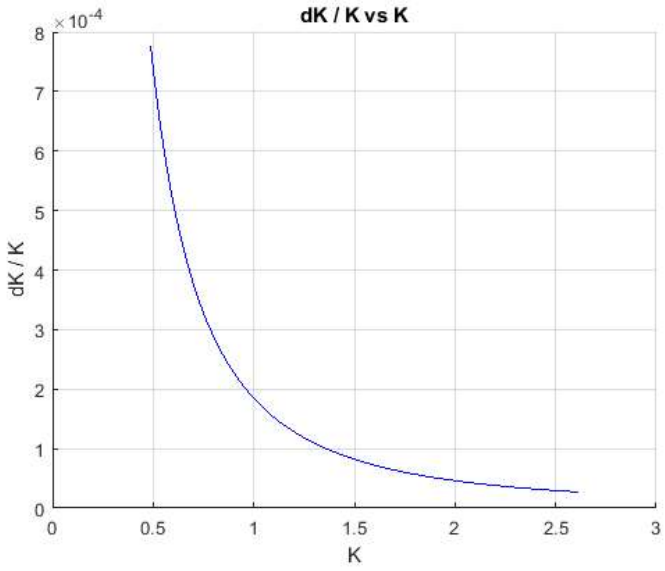

Figure 1: Relative change in K as a function of K for a 0.2 G change in the background field.

mm operating gap range of the HXR undulators. At small K, the relative change in K far exceeds the tolerance.

The phase advance through the cell is affected by the additional path length of the curved trajectory. From equation 16, the change in slippage from the added trajectory curvature is

$$\delta S = \left(\frac{e}{\gamma m v_z} b_0\right)^2 \frac{1}{3}\left(\frac{L}{2}\right)^3 \tag{22}$$

The change in cell phase is

$$\begin{aligned} \delta\Phi &= \frac{2\pi}{\lambda_r}\delta S & (23)\\ &= 2\pi \frac{2\gamma^2}{\lambda_u\left(1+\frac{1}{2}K^2\right)}\left(\frac{e}{\gamma m v_z} b_0\right)^2 \frac{1}{3}\left(\frac{L}{2}\right)^3 & (24)\\ &= \frac{\pi}{6\lambda_u\left(1+\frac{1}{2}K^2\right)}\left(\frac{e}{m v_z} b_0\right)^2 L^3 & (25) \end{aligned}$$

The smaller the K value, the larger the change in cell phase. In figure 2 we plot the change in cell phase over the HXR undulator operating range of K. We assume $b_0 = 0.2$ G over the length between BPMs of $L = 4.012667$ m. The tolerance on knowing the cell phase is far exceeded at small K.

We can add simulated external fields in the measurement analysis software to further study their effect. We add 0.2 G to B_x and look at the undulator parameter changes. Figure 3 shows the beam trajectory in HXU-031 at 20 mm gap in the laboratory after tuning. The trajectory has been corrected in software so the exit position at the location of the beam

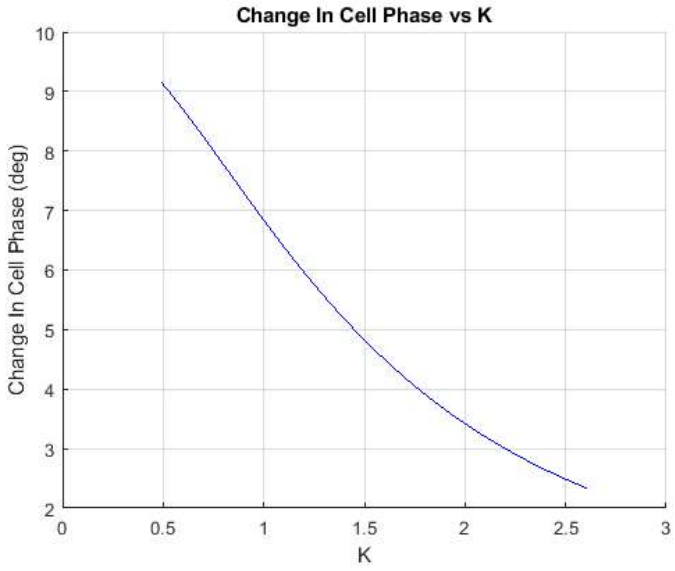

Figure 2: Change in cell phase for a 0.2 G field change over the range of HXR undulator K value.

position monitor is zero. The trajectory has some curvature, but the measured cell phase during the undulator calibration includes the effect of this curvature. If the undulator is moved to the tunnel and the background field difference between the tunnel and the laboratory produces a 0.2 G field difference on the beam axis, the exit position corrected trajectory changes to the one shown in figure 4. The curvature has increased. The changes to the analysis program results are

$$\begin{aligned}
\delta I_{1x} &= 80.2\ \mu\text{Tm} && (26)\\
\delta I_{2x} &= 161\ \mu\text{Tm}^2 && (27)\\
\delta \text{ Sagitta} &\simeq 3\ \mu\text{m} && (28)\\
\delta K &= 6.26 \times 10^{-4} && (29)\\
\delta K/K &= 13 \times 10^{-4} && (30)\\
\delta\Phi &= 10.99 \text{ deg} && (31)\\
\delta\phi_{rms} &= 1.76 \text{ deg} && (32)
\end{aligned}$$

The additional external field causes effects which far exceed the undulator tolerances.

The beam pipe corrector is used to apply an additional field to cancel the 0.2 G difference between the tunnel and the laboratory in order to restore the trajectory shown in figure 3 and to restore the undulator parameters to their calibrated values.

We can compare these results to the analytic calculations given above. For HXU-031

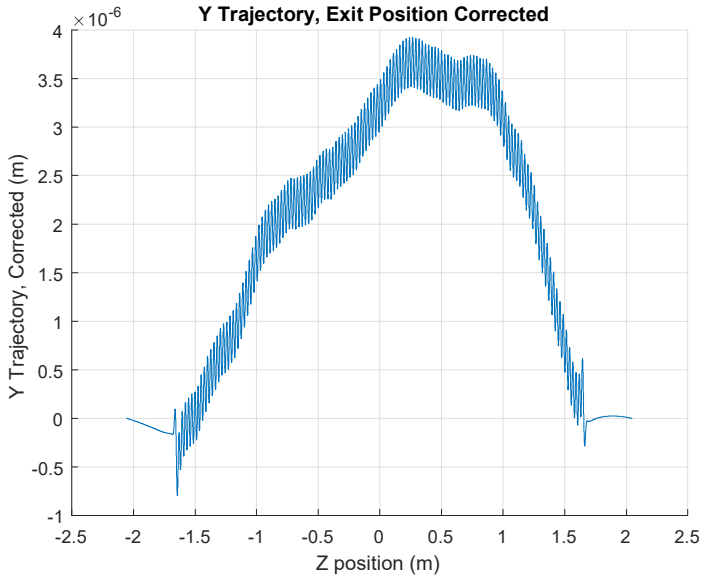

Figure 3: Trajectory in HXU-031 at 20 mm gap.

at 20 mm gap, we have the following parameters:

$$\lambda_u = 0.026 \text{ m} \tag{33}$$
$$K = 0.486417 \tag{34}$$
$$L = 4.012667 \text{ m} \tag{35}$$

For an external field of $b_0 = 0.2$ G on the beam axis, we calculate the following values using the formulas above.

$$\delta I_{1x} = b_0 L = 80 \ \mu\text{Tm} \tag{36}$$
$$\delta I_{2x} = \frac{1}{2} b_0 L^2 = 160 \ \mu\text{Tm}^2 \tag{37}$$
$$\text{Sagitta} = 3.01 \ \mu\text{m} \tag{38}$$
$$\delta K = 3.797 \times 10^{-4} \tag{39}$$
$$\delta K/K = 7.805 \times 10^{-4} \tag{40}$$
$$\delta\Phi = 9.17 \text{ deg} \tag{41}$$

The calculated change in K is smaller than the value from the analysis program. (This comparison was made on other undulators and the results are sensitive to the shape of the tuned trajectory, as discussed above.) The other values agree with the simulation. The conclusion is that the change in background field between the laboratory and the tunnel can cause changes from the calibrated undulator parameters that far exceed the tolerances. The beam pipe corrector is necessary, especially at the short wavelength end of the operating range.

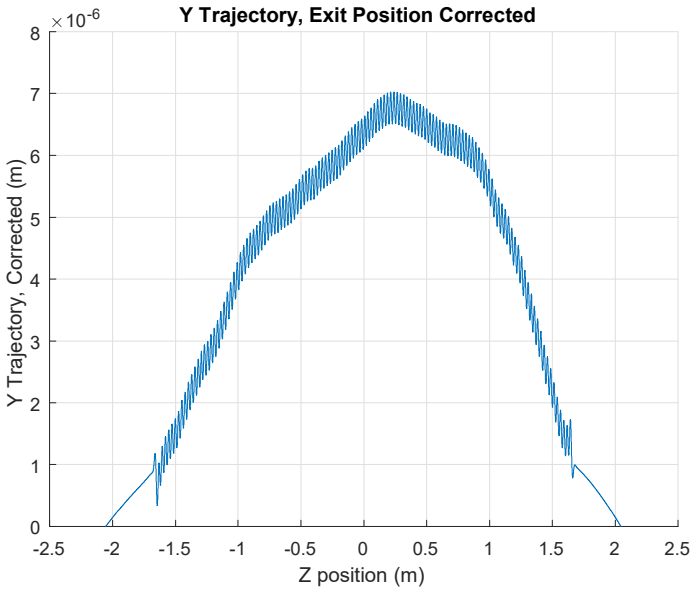

Figure 4: Trajectory in HXU-031 at 20 mm gap with an external field of 0.2 G on the beam axis.

4 Field Differences Between The Tunnel And The Laboratory

The magnetic fields in the laboratory and in the tunnel have been mapped [3]. The background fields measured at the SXR undulator bench are shown in figure 5. The background fields in the tunnel at the locations of the SXR undulators are shown in figure 6. The difference in the fields is shown in figure 7. Differences up to 0.18 G are evident.

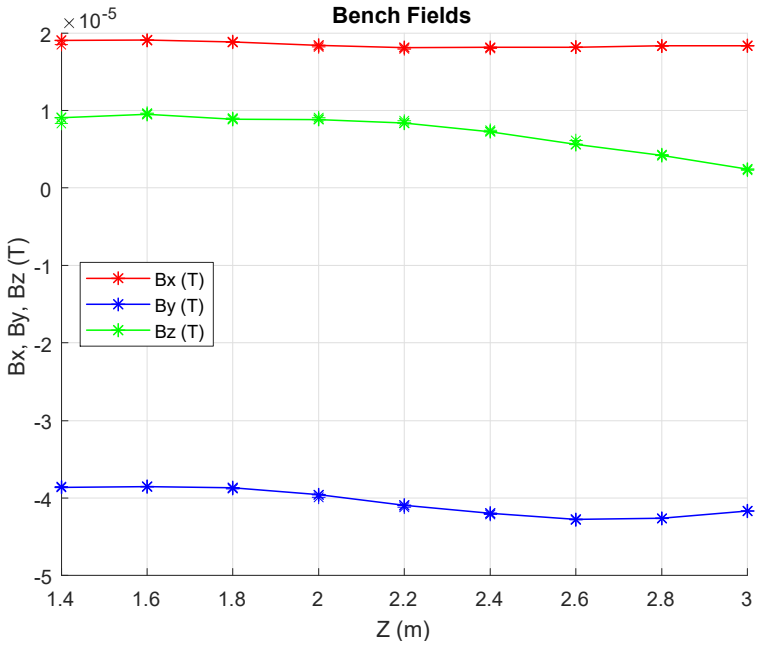

Figure 5: Field measurements at the SXR undulator bench.

[3] S. Anderson, "Earth's Field Measurements For The LCLS-II Undulator Lines And MMF Benches", April, 2020.

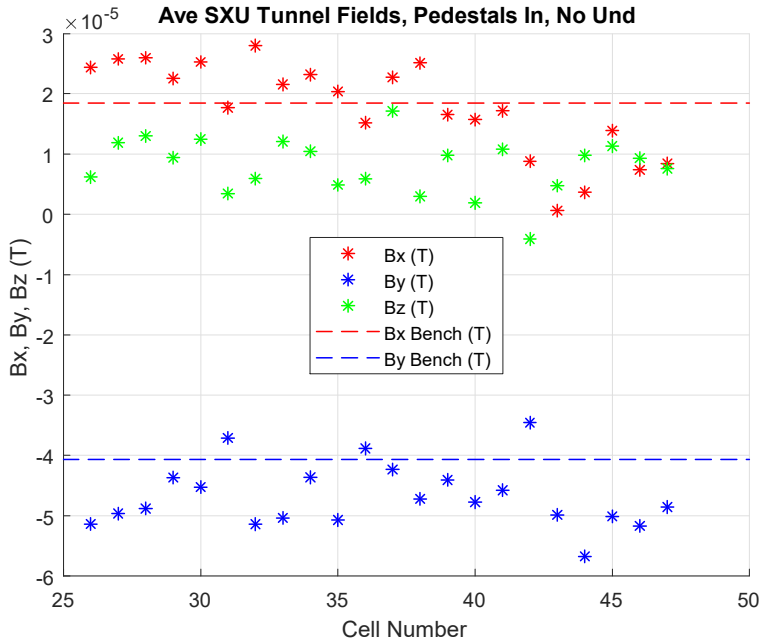

Figure 6: Measured magnetic field in the tunnel and at the measurement benches for the SXR undulators.

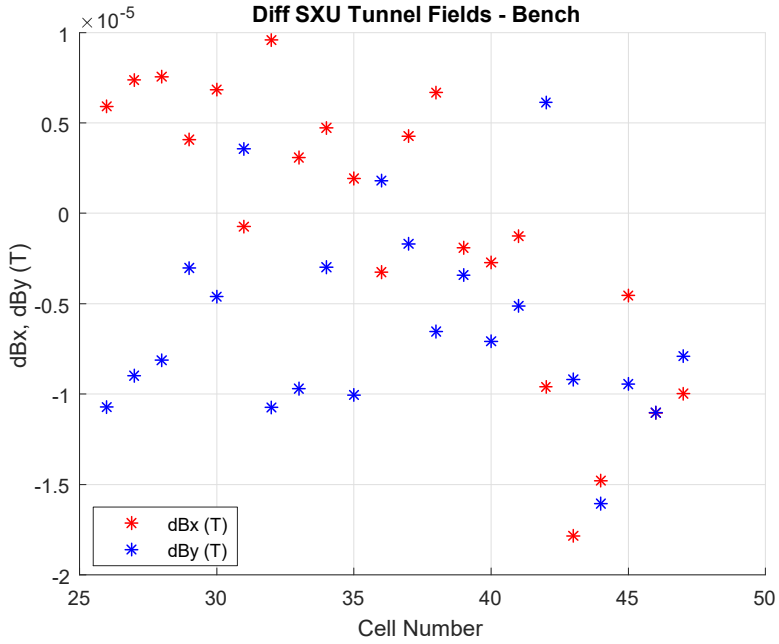

Figure 7: Field difference between the tunnel and the measurement bench for the SXR undulators.

The fields measured at the HXR undulator bench are shown in figure 8. The fields in

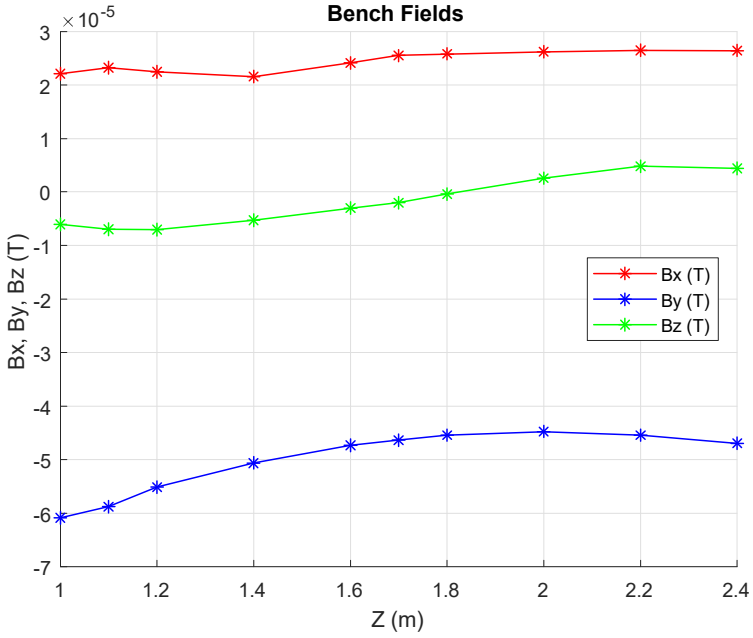

Figure 8: Fields measured at the HXR undulator bench.

the tunnel at the locations of the HXR undulators are shown in figure 9. The difference in the fields is shown in figure 10. Differences up to 0.24 G are evident.

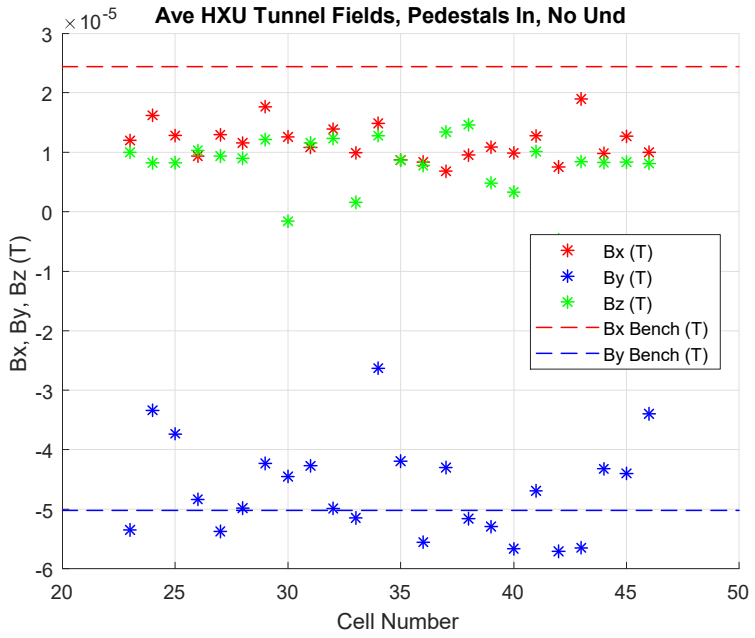

Figure 9: Measured magnetic field in the tunnel and at the measurement benches for the HXR undulators.

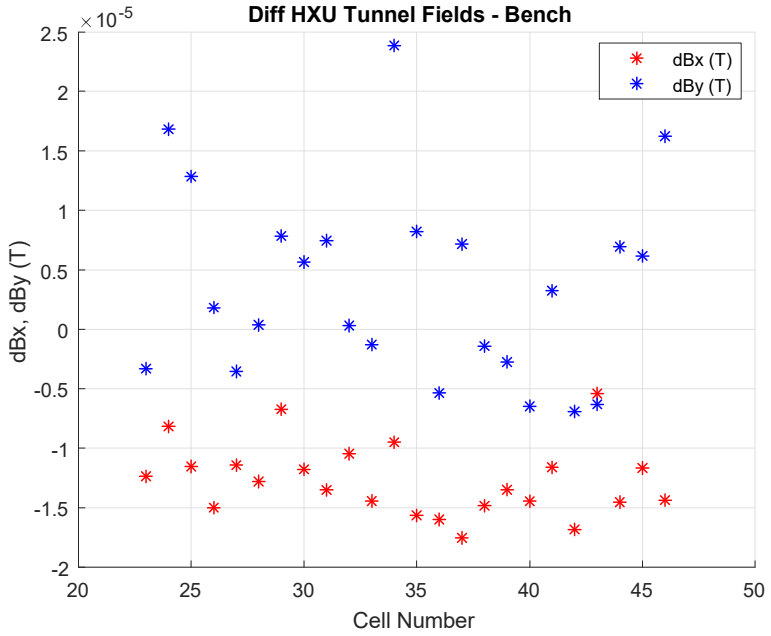

Figure 10: Field difference between the tunnel and the measurement bench for the HXR undulators.

5 Measurement Setup

In order to measure the effect of an external field on an undulator, we need to apply an external field in the measurement laboratory. We do this using a large Helmholtz coil. The Helmholtz coil surrounds the undulator, which has a beam pipe with correction coils inside it. The field inside the beam pipe is measured with a vibrating wire system[4] which gives the first and second integrals of B_x and B_y.

5.1 Helmholtz Coil

A large Helmholtz coil was used to make changes to the background field of the undulators. Figure 11 shows the Helmholtz coil assembled around SXU-021 and its measurement bench. The coil is built by adding windings to an aluminum truss frame. Great care was

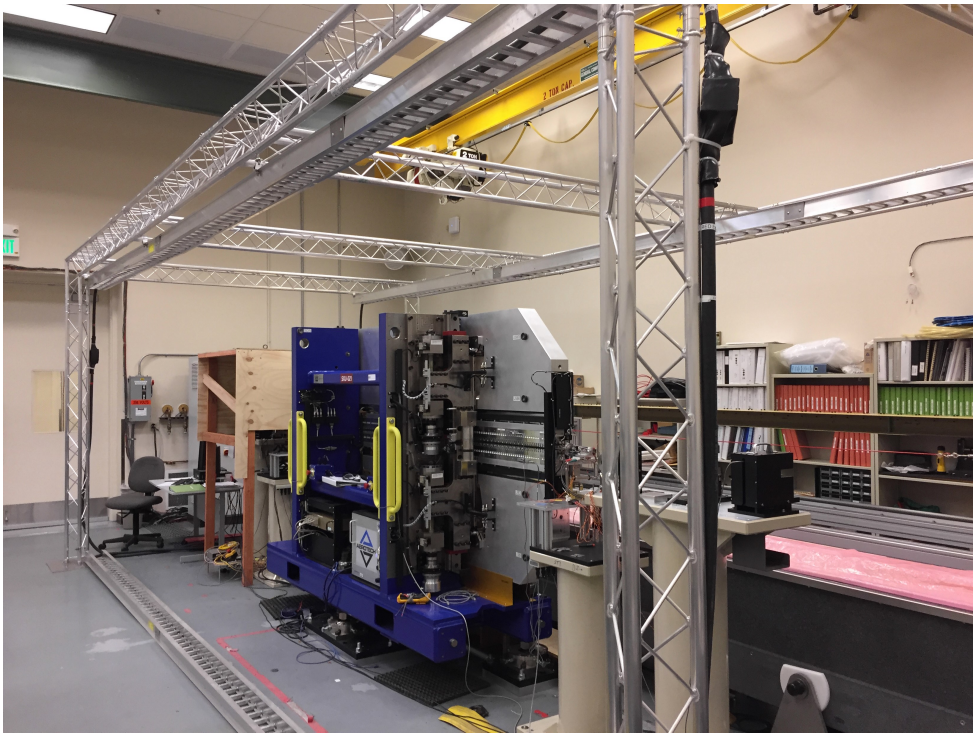

Figure 11: Large Helmholtz coil used to make changes to the background field of SXU-021.

required not to damage the granite measurement bench during assembly of the Helmholtz coil. Protective covers were left in place during the measurements. Figure 12 shows the Helmholtz coil assembled around HXU-031.

The beam line of the undulators is roughly 1.4 m above the floor. This set the size of the Helmholtz coil. The cables in the coil are placed in a square 2.8 m on a side centered on the beam line. A diagram of the setup is shown in figure 13.

[4] "A study of undulator magnets characterization using the vibrating wire".
Alexander Temnykh, Yurii Levashov, Zachary Wolf Nucl. Instr. and Meth. 622 (2010) 650

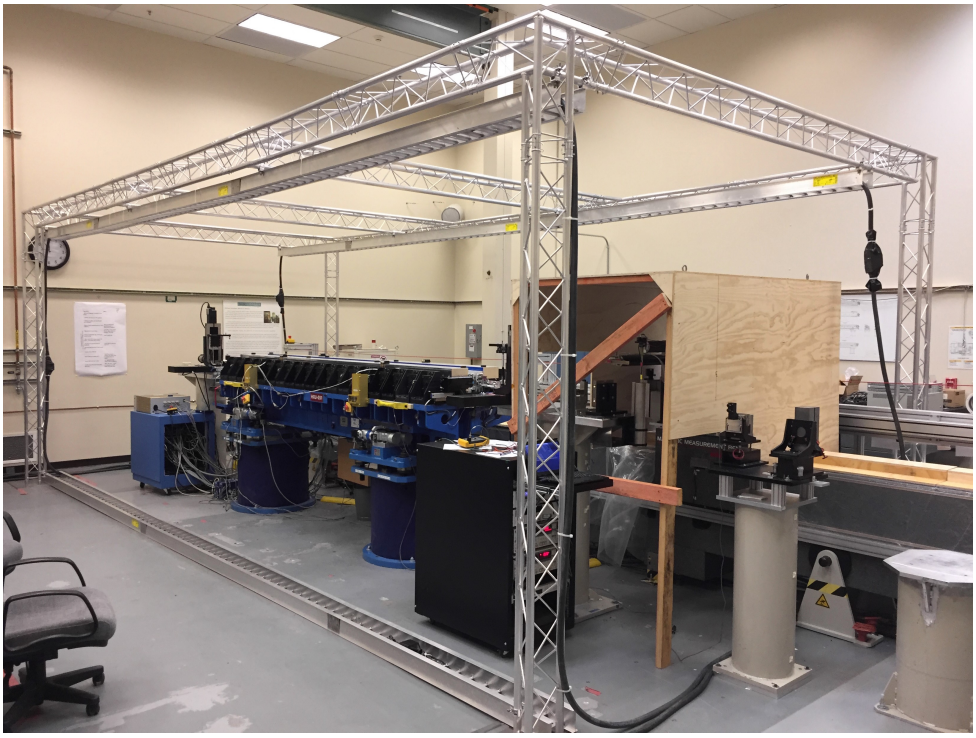

Figure 12: Helmholtz coil assembled around HXU-031.

Two power supplies are used to generate a magnetic field up to 0.5 G in any direction. The wiring diagram is illustrated in figure 14. The polarities of the currents in the windings are given in figure 15. The coils are wired so that coil 1 produces a field in the +x, +y (quadrant 1) direction. Coil 2 produces a field in the -x, +y (quadrant 2) direction. The coil currents I_1 and I_2 are combined with the same magnitude but opposite sign to give I_x which produces a B_x field, and with the same magnitude and same sign to give I_y which produces a B_y field. The relations between the currents and the fields are shown in the figure. The coordinate system has +z in the beam direction, +y up, and +x makes a right handed system.

The simple geometry makes it easy to calculate the field from the Helmholtz coil. For the current configuration in the figure which makes a B_x field, with 100 A in each cable, the field is

$$B_x = \frac{\mu_0 I}{2\pi r}\frac{1}{\sqrt{2}}4 \tag{42}$$

where $r = (d/2)\sqrt{2}$ and d is the 2.8 m width of the coil. The factor $1/\sqrt{2}$ comes from the field from each conductor being at 45 degrees with respect to the horizontal. The factor of 4 comes from the four conductors. Putting in numbers, and realizing that B_y behaves in the same way, we find

$$B_x = 0.2857 \text{ G / } 100 \text{ A} \tag{43}$$

$$B_y = 0.2857 \text{ G / } 100 \text{ A} \tag{44}$$

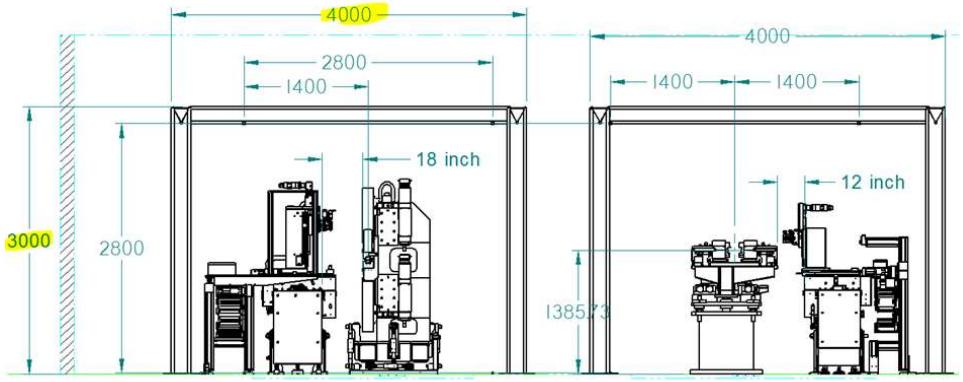

Figure 13: Diagram of the Helmholtz coil around each of the Kugler benches.

where the 100 A is the I_x or I_y indicated in the wiring diagram.

The field from the Helmholtz coil with no undulator was modeled. With $I_x = 100$ A producing a B_x field in an infinitely long coil in z, the uniformity of B_x vs x at $y = 0$ is shown in figure 16. The field is uniform at the 5% level over $x = \pm 0.5$ m. The uniformity of B_x vs y at $x = 0$ is shown in figure 17.

The Helmholtz coil was originally assembled in a storage area. A map of the B_x field uniformity in the z-direction was made. The map with $I_x = 200$ A is shown in figure 18. The field is uniform over the 3.4 meter length of the undulators. For this configuration, the cables went straight down the supports at the end of the Helmholtz coil. We also tried configuring the cables in an "X" shape at the ends. This gave large fields on the beam axis at the ends. The configuration with the cables going down the supports was chosen as the more favorable.

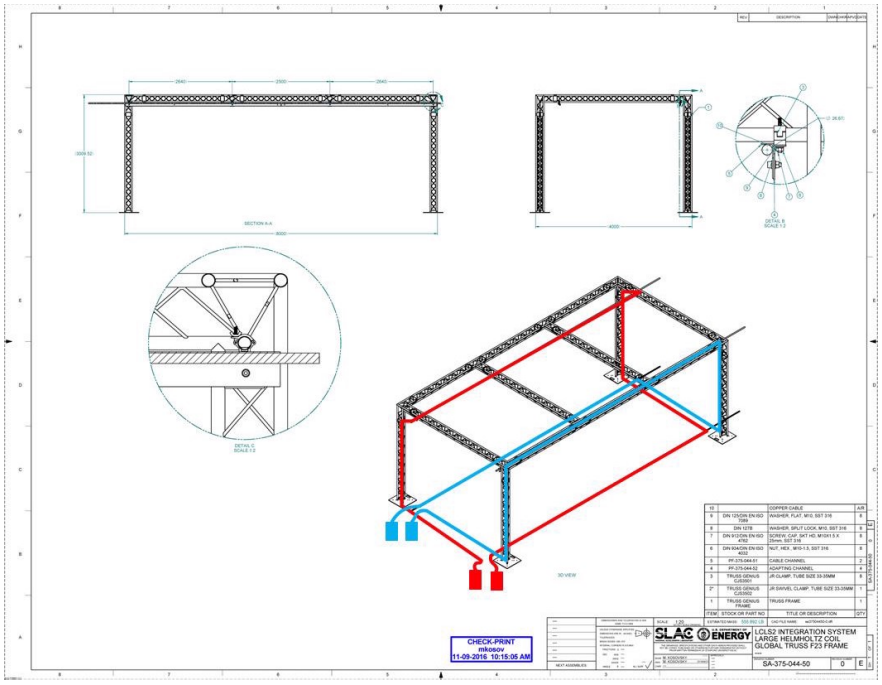

Figure 14: Wiring diagram for the Helmholtz coil.

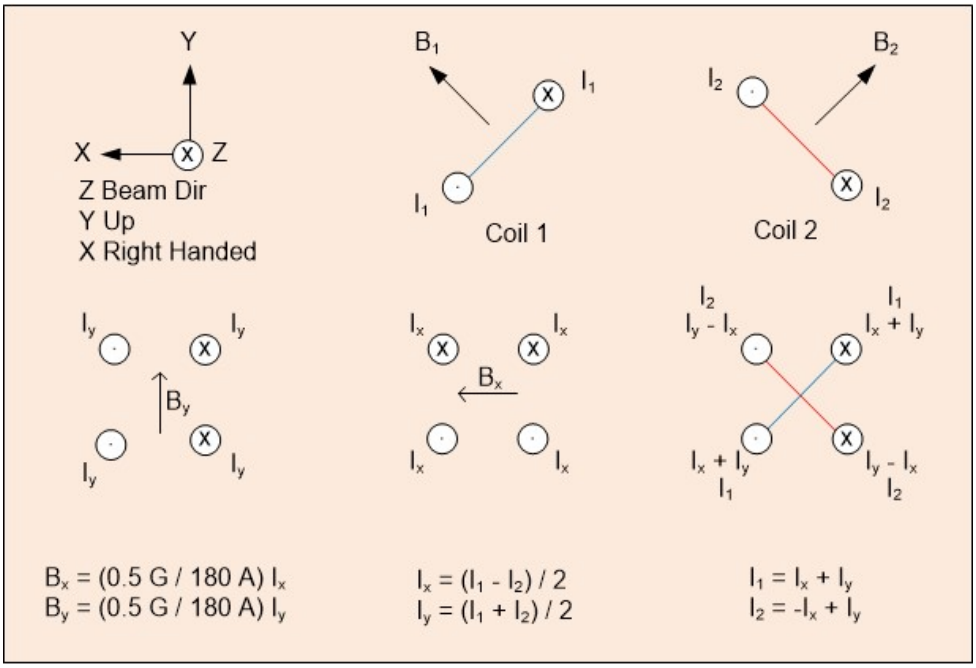

Figure 15: Polarity of the currents in the windings. The measured field in the Helmholtz coil for given current is indicated.

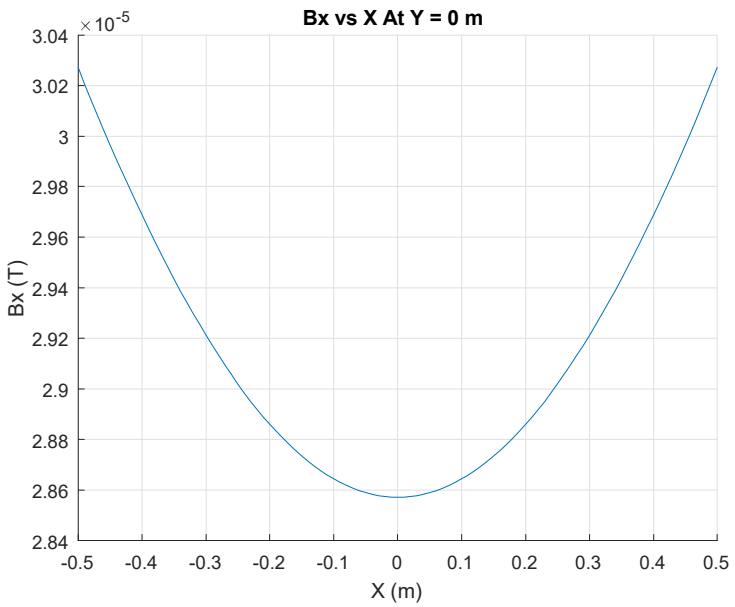

Figure 16: B_x vs x with $I_x = 100$ A.

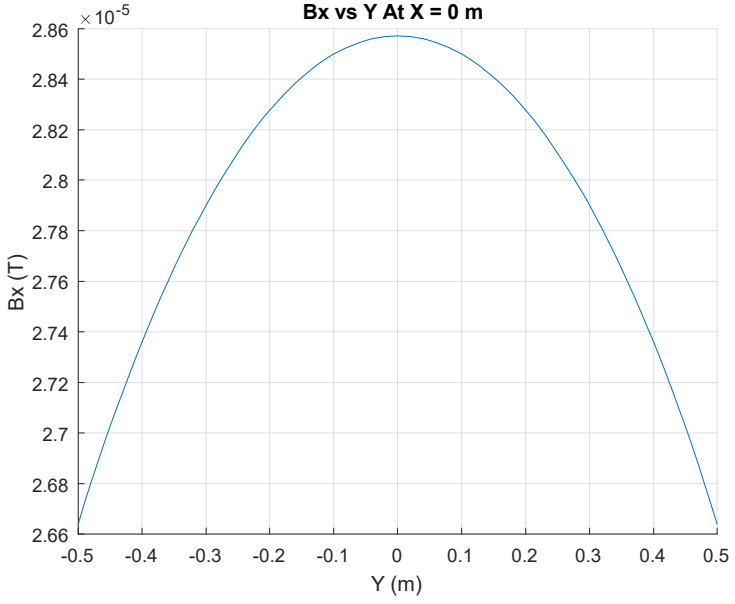

Figure 17: B_x vs y with $I_x = 100$ A.

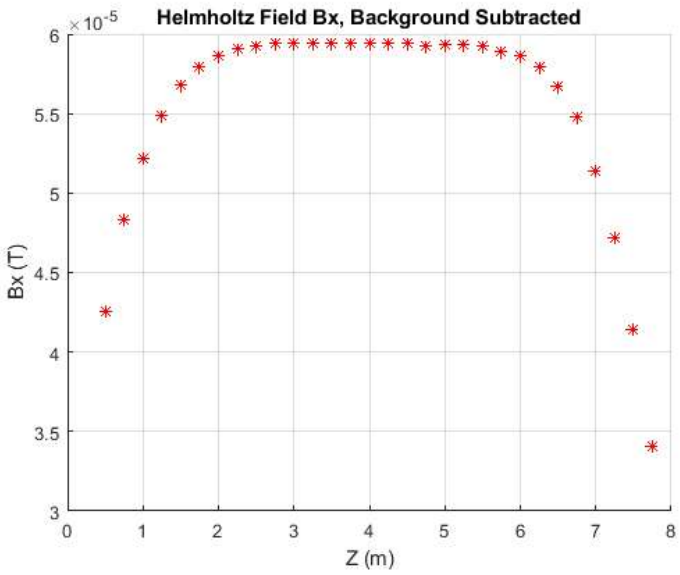

Figure 18: B_x vs z at $x = 0$ and $y = 0$ with $I_x = 200$ A.

5.2 Beam Pipe Corrector

The SXU and HXU beam pipes have a rectangular array of windings in them in a manner similar to the Helmholtz coil. Figure 19 shows a drawing of the HXR undulator beam pipe and figure 20 shows a photo[5].

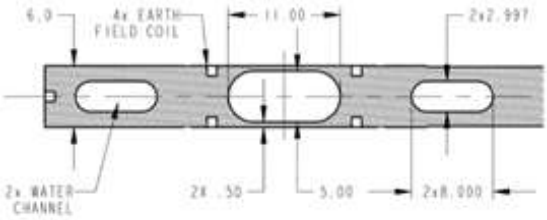

Figure 19: Drawing of the HXR undulator beam pipe.

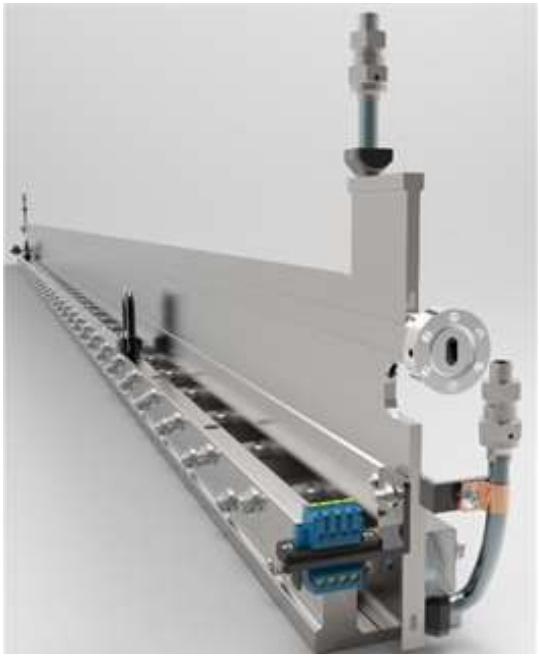

Figure 20: Photo of the HXR undulator beam pipe.

The beam pipe corrector coils for both the SXR and HXR undulators are placed with the wire centers on a rectangular grid 14.5 mm by 5.0 mm. The diagonal wires are connected so that they produce two coils. A wiring diagram for both the SXR and HXR coils is shown in figure 21. For both the SXR and HXR beam pipes, the coils are wired so that coil 1

[5] J. Lerch, et al, "Design Of the HGVPU Undulator Vacuum Chamber For LCLS-II", Proceedings of NAPAC2016, Chicago, IL.

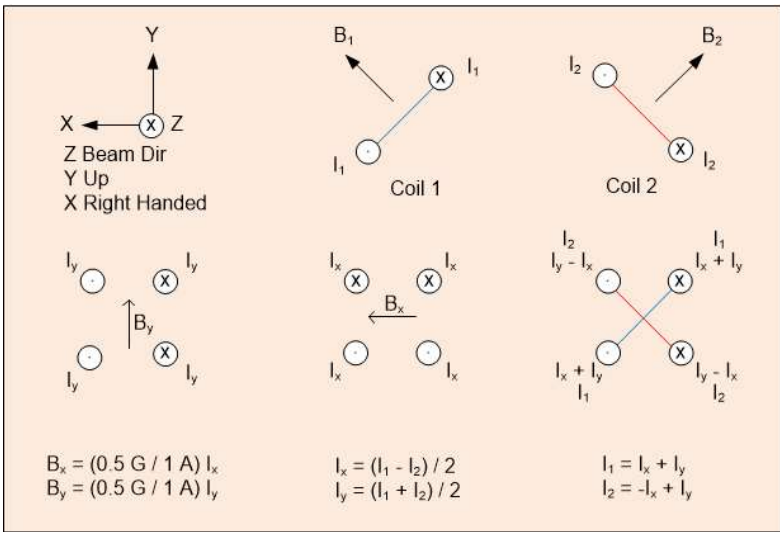

Figure 21: Wiring diagram for the SXR and HXR beam pipe correctors.

produces a field in the +x, +y (quadrant 1) direction. Coil 2 produces a field in the -x, +y (quadrant 2) direction. The coil currents I_1 and I_2 are combined with the same magnitude but opposite sign to give I_x which produces a B_x field, and with the same magnitude and same sign to give I_y which produces a B_y field. The relations between the currents and the fields are shown in the figure. The coordinate system has +z in the beam direction, +y up, and +x makes a right handed system. The transfer functions given in the figure are very rough, and in fact they are gap dependent and different for the SXR and HXR beam pipes. The transfer functions will be discussed below. The SXR beam pipe has the long dimension of the coil horizontal and the HXR beam pipe has the long dimension vertical.

The fields from the beam pipe corrector were simulated. For the HXR beam pipe, when $I_x = 1$ A, the field B_x as a function of undulator gap is shown in figure 22. The reason for the gap dependence is the steel undulator poles. The steel poles were modeled to have infinite permeability. They produced image currents which were modeled as the current in the corrector multiplied by the fraction of steel poles in the magnet array. Successive images up to the 10'th image current were successively multiplied by this fraction. The trim winding currents and their images reflected in the vertical poles at 20 mm gap are shown in figure 23. Notice how the image currents all have the same sign at given y and enhance the field as the gap is closed.

When a current $I_y = 1$ A was modeled in the windings, the field B_y as a function of gap shown in figure 24 was the result of the model. In this case the currents in the windings at fixed y have opposite signs. This produces cancellations in the image currents resulting in the field decreasing at small gap. The alternating sign image currents reflected in the vertical poles at 20 mm gap are shown in figure 25.

The modeled fields are provided as a reference. The measured fields given in the following sections look similar. The modeled fields showing the effect of the image currents help to explain the shape of the curves.

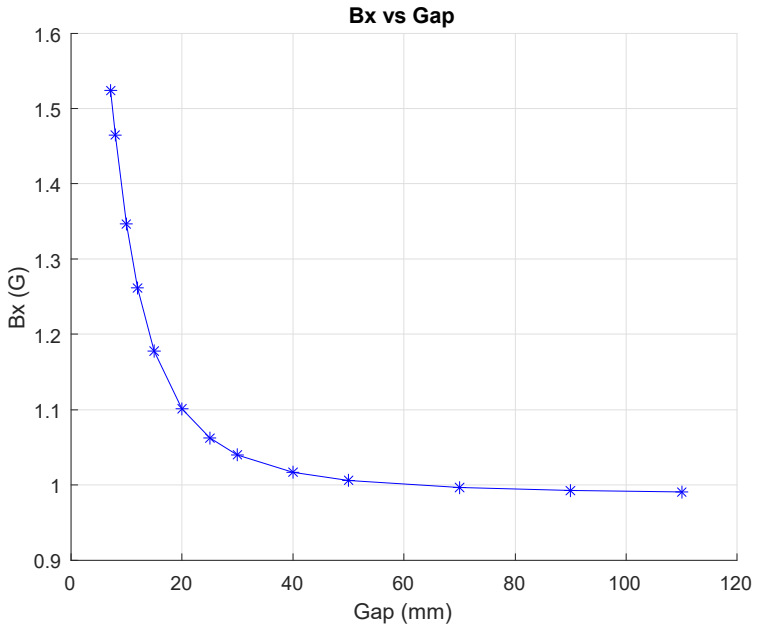

Figure 22: Simulated field B_x as a function of undulator gap when $I_x = 1$ A.

With no steel poles, the model gives for the HXR beam pipe corrector

$$B_x = 0.9862 \text{ G} / 1 \text{ A} \quad (45)$$
$$B_y = 0.3401 \text{ G} / 1 \text{ A} \quad (46)$$

and for the SXR beam pipe corrector

$$B_x = 0.3401 \text{ G} / 1 \text{ A} \quad (47)$$
$$B_y = 0.9862 \text{ G} / 1 \text{ A} \quad (48)$$

The measurements should approach these values at large gaps.

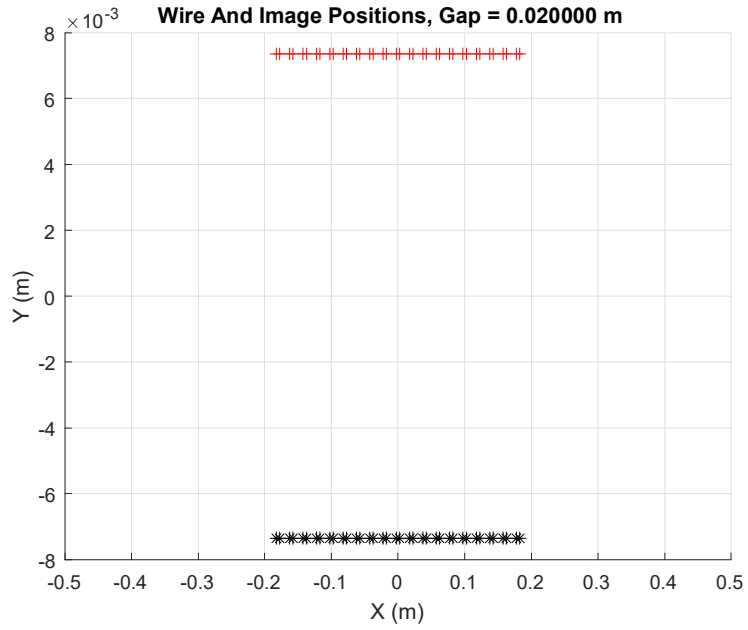

Figure 23: Corrector currents and image currents for I_x at 20 mm gap.

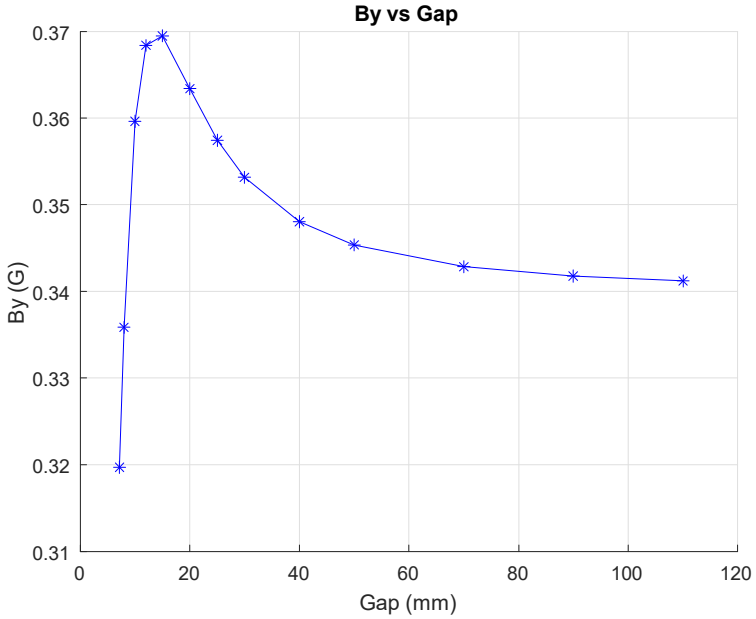

Figure 24: Simulated field B_y as a function of undulator gap when $I_y = 1$ A.

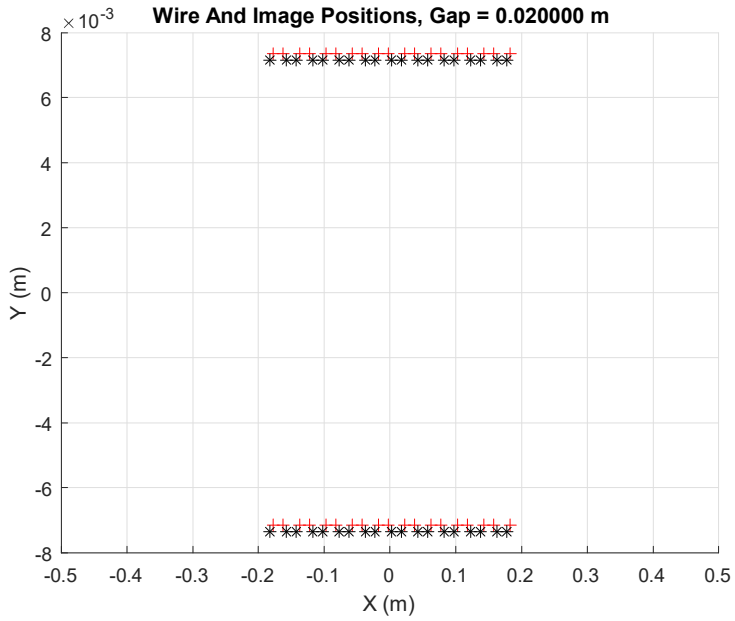

Figure 25: Corrector currents and image currents for I_y at 20 mm gap.

6 Test Plan

6.1 Measure The Effect Of An External Applied Field

The measured difference in the background fields between the tunnel and the laboratory was discussed above. Field differences up to $\sim$ 0.25 G are present. Based on these measurements, we set the range of background field differences for these tests from -0.3 G to $+0.3$ G. We must also study the gap dependence of the effects of the external fields. The test plan is as follows:

1. Assemble the Helmholtz coil around a test bench and undulator.
2. Install a vibrating wire field integral measurement system in a beam pipe. The beam pipe contains the trim windings.
3. Place the beam pipe with vibrating wire system and trim windings in the undulator. Align the beam pipe so the trim windings and vibrating wire are centered on the beam axis.
4. Define a set of undulator gaps to perform measurements at. For the SXR undulators, measure at gaps of 7.2, 8, 10, 12, 16, 20, $25, 40, 70, 100, 140, 180$ mm. For the HXR undulators, measure at gaps of 7.2, 8, 10, 12, 16, 20, $25, 30, 40, 110$ mm.
5. Define a set of measurements to perform at each undulator gap. For both SXR and HXR undulators, measure the field integrals I_{1x}, I_{1y}, I_{2x}, I_{2y} at each undulator gap using the vibrating wire system.
6. With no current in the Helmholtz coil, measure the field integrals at the undulator gaps.
7. Using the Helmholtz coil, apply a B_x field of 0.3 G. Measure the field integrals at a gap of 10 mm. Verify that the B_y field integrals do not change.
8. Using the Helmholtz coil, apply a B_y field of 0.3 G. Measure the field integrals at a gap of 10 mm. Verify that the B_x field integrals do not change.
9. Using the Helmholtz coil, apply B_x fields of $0.0, 0.1, 0.2, 0.3$ G. Measure the field integrals at the undulator gaps.
10. Using the Helmholtz coil, apply B_y fields of $0.0, 0.1, 0.2, 0.3$ G. Measure the field integrals at the undulator gaps.
11. Analyze the measurements at $0.0, 0.1, 0.2, 0.3$ G to verify that the field integral variation depends linearly on the applied field at each undulator gap. Determine the two response coefficients dI_{1x}/dB_x and dI_{1y}/dB_y at each undulator gap.
12. Perform a spline fit to the gap dependence of the field integral response coefficients. Make a file of spline points fitting dI_{1x}/dB_x vs gap, and the same for dI_{1y}/dB_y vs gap.

6.2 Measure The Response Of The Beam Pipe Correctors

Determine how the beam pipe correctors behave at different undulator gaps. The measurement plan to do this is as follows:

1. Turn off the Helmholtz coil so no additional external fields are applied.

2. Define a set of undulator gaps to perform measurements at. For the SXR undulators, measure at gaps of 7.2, 8, 10, 12, 16, 20, 25, 40, 70, 100, 140, 180 mm. For the HXR undulators, measure at gaps of 7.2, 8, 10, 12, 16, 20, 25, 30, 40, 110 mm.

3. Define a set of measurements to perform at each undulator gap. For both SXR and HXR undulators, measure the field integrals I_{1x}, I_{1y}, I_{2x}, I_{2y} at each undulator gap using the vibrating wire system.

4. Apply a current of 1 Amp making a B_x field in the beam pipe corrector with an undulator gap of 10 mm. Verify that the B_y field integrals do not change.

5. Apply a current of 1 Amp making a B_y field in the beam pipe corrector with an undulator gap of 10 mm. Verify that the B_x field integrals do not change.

6. Apply currents of $I_x = -1.0, -0.5, 0.0, 0.5, 1.0$ A making a B_x field in the beam pipe corrector. Measure the field integrals at the undulator gaps.

7. Apply currents of $I_y = -1.0, -0.5, 0.0, 0.5, 1.0$ A making a B_y field in the beam pipe corrector. Measure the field integrals at the undulator gaps.

8. Analyze the measurements at $-1.0, -0.5, 0.0, 0.5, 1.0$ A to verify that the field integrals vary linearly with the applied current at each undulator gap. Determine the two response coefficients dI_{1x}/dI_x and dI_{1y}/dI_y at each undulator gap.

9. Perform a spline fit to the gap dependence of the field integral response coefficients. Make a file of spline points fitting dI_{1x}/dI_x vs gap, and the same for dI_{1y}/dI_y vs gap.

6.3 Calibration Of The Beam Pipe Correctors

In the following sections the symbols used for currents are I_x and I_y. The symbols used for first field integrals are I_{1x} and I_{1y}. The context and units should prevent confusion, but the similarity of the symbols must be noted.

At this point, the change in undulator field integral for a given external applied field is known. These are the fits to dI_{1x}/dB_x and dI_{1y}/dB_y as a function of gap. For a given field difference between the tunnel and the lab ΔB, the response parameter times the field difference gives the change in the undulator field integral at a given undulator gap g.

$$\Delta I_{1x}(g) = \frac{dI_{1x}}{dB_x}(g)\ \Delta B_x \tag{49}$$

$$\Delta I_{1y}(g) = \frac{dI_{1y}}{dB_y}(g)\ \Delta B_y \tag{50}$$

We also know the change in undulator field integral for a given current in the beam pipe corrector windings as a function of undulator gap. These are the fits to dI_{1x}/dI_x and dI_{1y}/dI_y as a function of gap. For a given current I_x or I_y, the response parameter times the current gives the change in the undulator field integral at a given undulator gap g.

$$\Delta I_{1x}(g) = \frac{dI_{1x}}{dI_x}(g)\ I_x \tag{51}$$

$$\Delta I_{1y}(g) = \frac{dI_{1y}}{dI_y}(g)\ I_y \tag{52}$$

Combining these results, for given external field difference between the tunnel and the lab, we know the change in the undulator field integrals. We can set the trim current to give the negative of the change of the undulator field integral. In this way, the field integral has the same value it had in the lab during calibration.

$$\frac{dI_{1x}}{dI_x}(g)\ I_x = -\frac{dI_{1x}}{dB_x}(g)\ \Delta B_x \tag{53}$$

$$\frac{dI_{1y}}{dI_y}(g)\ I_y = -\frac{dI_{1y}}{dB_y}(g)\ \Delta B_y \tag{54}$$

We arrive at the trim winding current settings to cancel an applied external field:

$$I_x = -\frac{\frac{dI_{1x}}{dB_x}(g)}{\frac{dI_{1x}}{dI_x}(g)}\Delta B_x \tag{55}$$

$$I_y = -\frac{\frac{dI_{1y}}{dB_y}(g)}{\frac{dI_{1y}}{dI_y}(g)}\Delta B_y \tag{56}$$

After the calibrations have been performed, this procedure should be tested by applying a range of external fields and setting the current in the trim windings to cancel the effect on the field integrals from the applied fields. Measure the field integrals to verify that the values are the same as with zero applied field.

7 Measurements

In this section we first demonstrate that the small changes in the background field and the small field from the corrector coils cause a linear change in the field integrals. We then give the measured responses to the field integrals as a function of gap. Finally, we give the calibration values.

As a check on the Helmholtz coil measurements, we calculate the field integral response at large gap where there is minimal influence from the steel poles. At large gap, when the Helmholtz coil makes a field change dB_x, the field integral change should be $dI_{1x} = dB_x L$, where L is the length of the vibrating wire. So $dI_{1x}/dB_x = L$. The length of the vibrating wire is approximately $L = 3.6$ m. A similar relation applies for dI_{1y}. At large gaps, the external field response functions should have the following values

$$\frac{dI_{1x}}{dB_x} = 360\ \mu\text{Tm} \ / \ \text{G} \tag{57}$$

$$\frac{dI_{1y}}{dB_y} = 360\ \mu\text{Tm} \ / \ \text{G} \tag{58}$$

A possible complication is the effect of the steel frame of the SXR undulator. This can affect the Helmholtz coil fields, so a modest deviation from these values would be acceptable for the SXR undulator. The HXR undulator, however, is built on an aluminum strongback which will not affect the Helmholtz coil fields, so these values should be accurate.

For a check on the beam pipe corrector measurements, we use the simulated fields with no steel poles. As given above, the simulation with no steel poles gives for the SXR beam pipe corrector

$$\frac{dB_x}{dI_x} = 0.3401\ \text{G} \ / \ \text{A} \tag{59}$$

$$\frac{dB_y}{dI_y} = 0.9862\ \text{G} \ / \ \text{A} \tag{60}$$

and for the HXR beam pipe corrector

$$\frac{dB_x}{dI_x} = 0.9862\ \text{G} \ / \ \text{A} \tag{61}$$

$$\frac{dB_y}{dI_y} = 0.3401\ \text{G} \ / \ \text{A} \tag{62}$$

The change in the field integral should be $dI_{1x} = dB_x L$, where $L = 3.6$ m is the length of the vibrating wire. A similar relation applies for dI_{1y}. For the SXR undulators, at large gap we have

$$\frac{dI_{1x}}{dI_x} = 122.44\ \mu\text{Tm} \ / \ \text{A} \tag{63}$$

$$\frac{dI_{1y}}{dI_y} = 355.03\ \mu\text{Tm} \ / \ \text{A} \tag{64}$$

and for the HXR undulators with the rotated beam pipe, at large gap we have

$$\frac{dI_{1x}}{dI_x} = 355.03\ \mu\text{Tm}\ /\ \text{A} \tag{65}$$

$$\frac{dI_{1y}}{dI_y} = 122.44\ \mu\text{Tm}\ /\ \text{A} \tag{66}$$

The steel from of the SXR undulator is far from the beam pipe and should not affect these results.

7.1 Linearity Of Response

When the Helmholtz coil applies an external field to the undulators, the measured field integrals change in a linear way. As an example, consider figure 26 which shows the response of HXU-031 at 10 mm gap to the applied field. A line is fit to the measured points and the slope of the line is the response parameter dI_{1x}/dB_x at 10 mm gap.

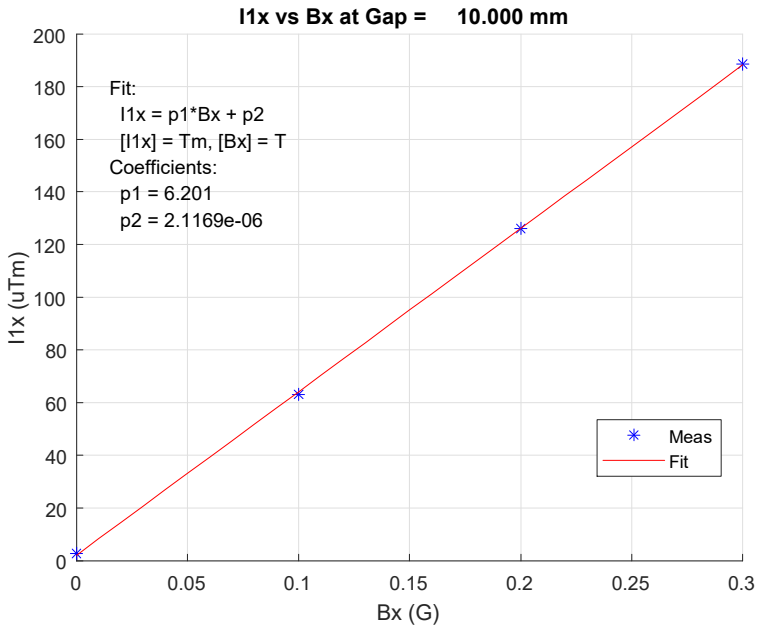

Figure 26: The measured field integral I_{1x} changes in a linear way with applied field B_x from the Helmholtz coil.

When the beam pipe corrector is energized, the measured field integrals change in a linear way with current in the coil. As an example, consider figure 27 which shows the response of HXU-031 at 10 mm gap to the applied current. A line is fit to the measured points and the slope of the line is the response parameter dI_{1x}/dI_x at 10 mm gap.

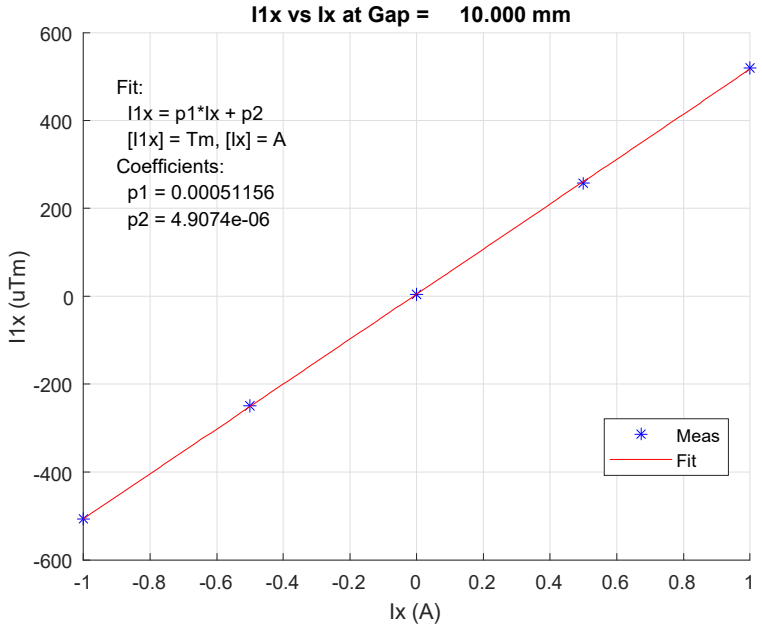

Figure 27: The measured field integral I_{1x} changes in a linear way with applied beam pipe corrector current I_x.

7.2 Measured Response To An Applied Field

7.2.1 SXU-021

The Helmholtz coil was set up around SXU-021 and external fields were applied. The field integrals were measured with different applied fields and the response functions dI_{1x}/dB_x and dI_{1y}/dB_y were measured at a number of undulator gaps according to the test plan given above. Figure 28 shows the measured response function dI_{1x}/dB_x as a function of gap. Also shown are the spline points and spline fit to the measurements. The measurements at large gap do not go to the predicted result of $dI_{1x}/dB_x = 360$ μTm / G, probably due to the steel frame of the undulator.

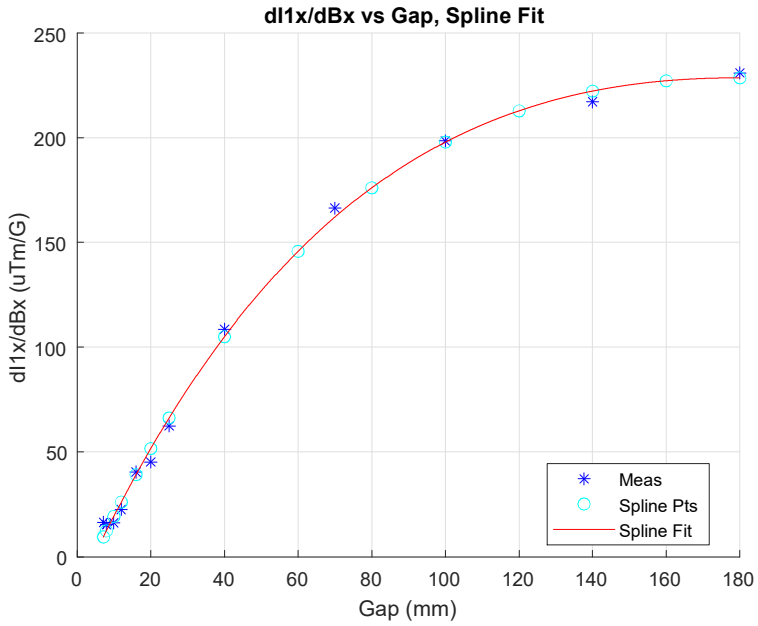

Figure 28: Response function dI_{1x}/dB_x as a function of gap for SXU-021.

Figure 29 shows the measured response function dI_{1y}/dB_y as a function of gap. Also shown are the spline points and spline fit to the measurements. The measurements at large gap do not go to the predicted result of $dI_{1y}/dB_y = 360$ μTm / G, probable due to the steel frame. The measurements do go to the same value as dI_{1x}/dB_x, as they should.

At small gap, the steel poles shield B_x from the gap and I_{1x} goes to zero. At small gap, the steel poles enhance I_{1y} by a factor of approximately 2.2.

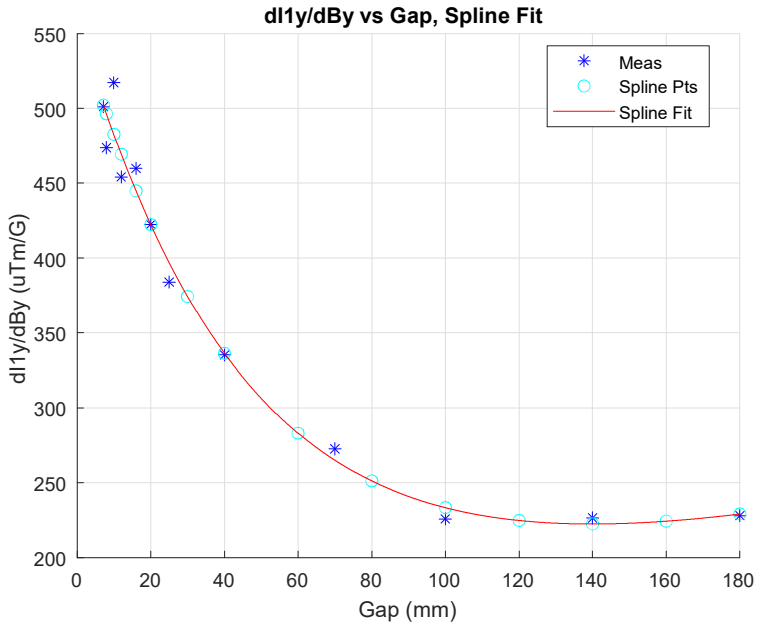

Figure 29: Response function dI_{1y}/dB_y as a function of gap for SXU-021.

7.2.2 HXU-031

Figure 30 shows the measured response function dI_{1x}/dB_x as a function of gap. Also shown are the spline points and spline fit to the measurements. The measurements at large gap go to the expected result of $dI_{1x}/dB_x = 360$ μTm / G.

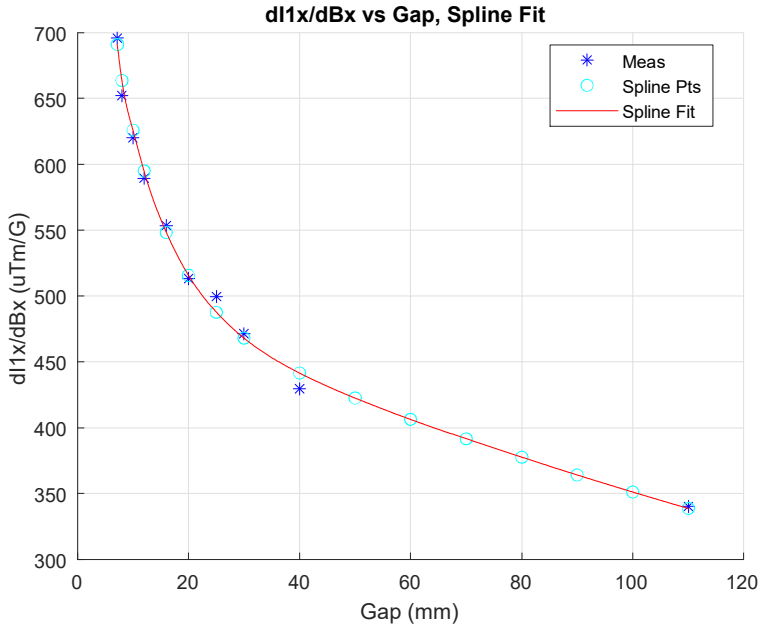

Figure 30: Response function dI_{1x}/dB_x as a function of gap for HXU-031.

Figure 31 shows the measured response function dI_{1y}/dB_y as a function of gap. Also shown are the spline points and spline fit to the measurements. The measurements at large gap go to the expected result of $dI_{1y}/dB_y = 360$ μTm / G.

At small gap, the steel poles shield B_y from the gap and I_{1y} goes to zero. The steel poles enhance I_{1x} by a factor of approximately 2.

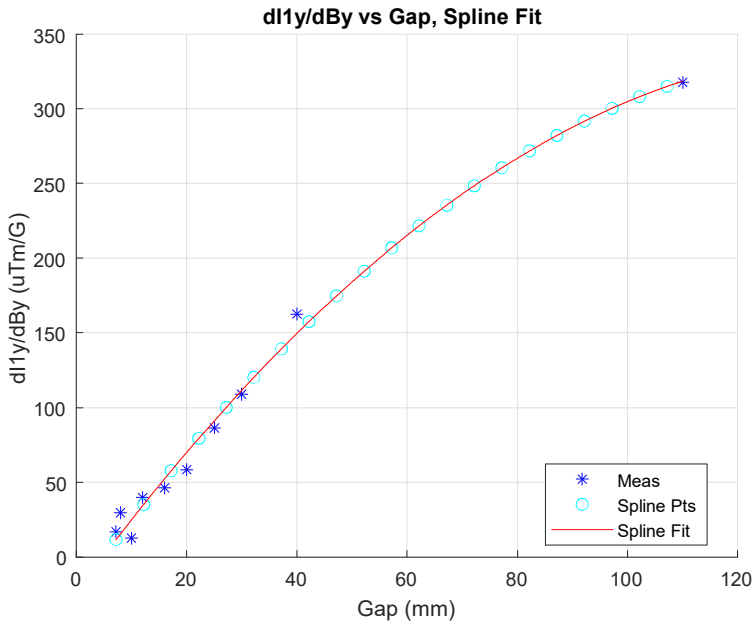

Figure 31: Response function dI_{1y}/dB_y as a function of gap for HXU-031.

7.3 Measured Response To The Beam Pipe Corrector

The gap dependence of the response functions for the beam pipe correctors are given below. The form of the gap dependence agrees with the model given previously. The numerical values are similar to the model, but differ at the 20% level. The disagreement most likely comes from the method of calculating the image currents using the simple fraction of steel in the magnet assemblies. The image current model, however, is very useful for understanding the shape of the response functions.

7.3.1 SXU-021

A beam pipe with correction coils was set up in SXU-021. The field integrals were measured with different coil currents and the response functions dI_{1x}/dI_x and dI_{1y}/dI_y were calculated at a number of undulator gaps according to the test plan given above. Figure 32 shows the measured response function dI_{1x}/dI_x as a function of gap. Also shown are the spline points and spline fit to the measurements. The measurements at large gap do not go to the expected result of $dI_{1x}/dI_x = 122.44$ μTm / A.

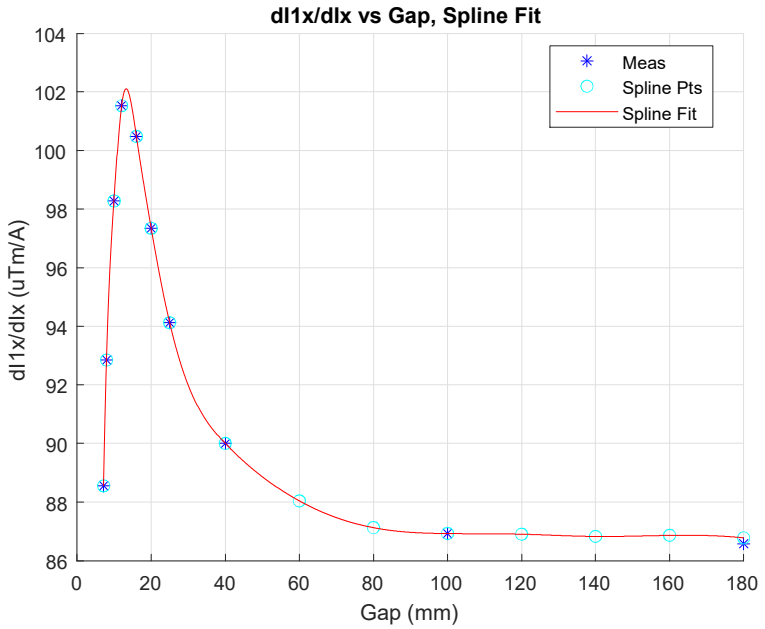

Figure 32: Response function dI_{1x}/dI_x as a function of gap for SXU-021.

Figure 33 shows the measured response function dI_{1y}/dI_y as a function of gap. Also shown are the spline points and spline fit to the measurements. The measurements at large gap are close to the expected result of $dI_{1y}/dI_y = 355.03$ μTm / A.

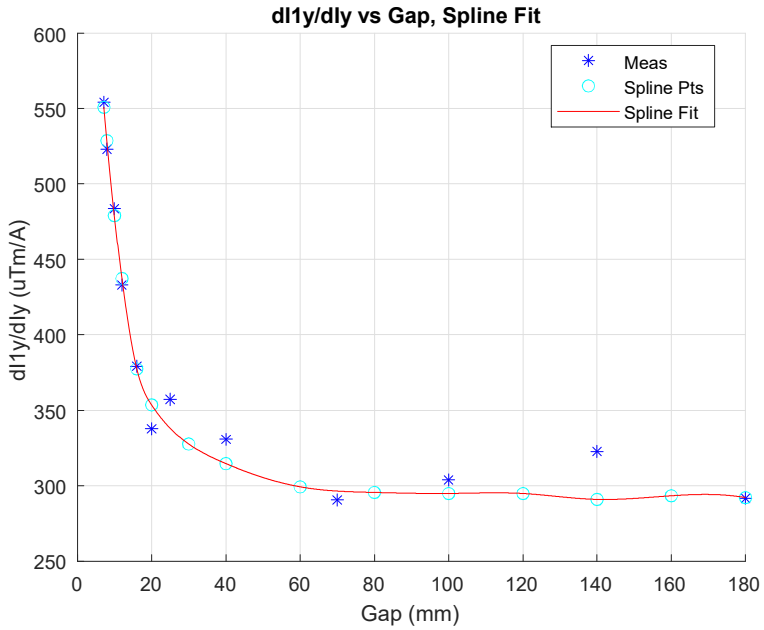

Figure 33: Response function dI_{1y}/dI_y as a function of gap for SXU-021.

7.3.2 HXU-031

Figure 34 shows the measured response function dI_{1x}/dI_x as a function of gap. Also shown are the spline points and spline fit to the measurements. The measurements at large gap are close to the expected result of $dI_{1x}/dI_x = 355.03$ μTm / A.

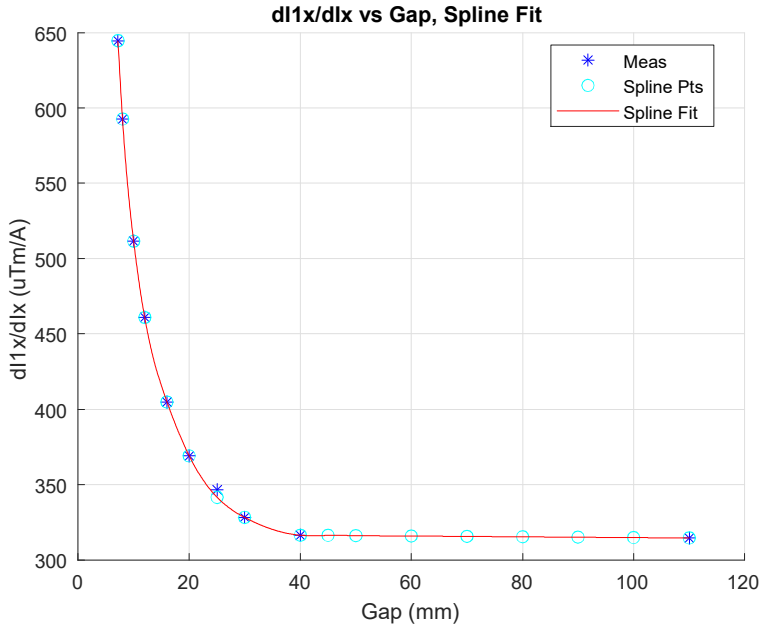

Figure 34: Response function dI_{1x}/dI_x as a function of gap for HXU-031.

Figure 35 shows the measured response function dI_{1y}/dI_y as a function of gap. Also shown are the spline points and spline fit to the measurements. The measurements at large gap agree with the expected result of $dI_{1y}/dI_y = 122.44$ μTm / A.

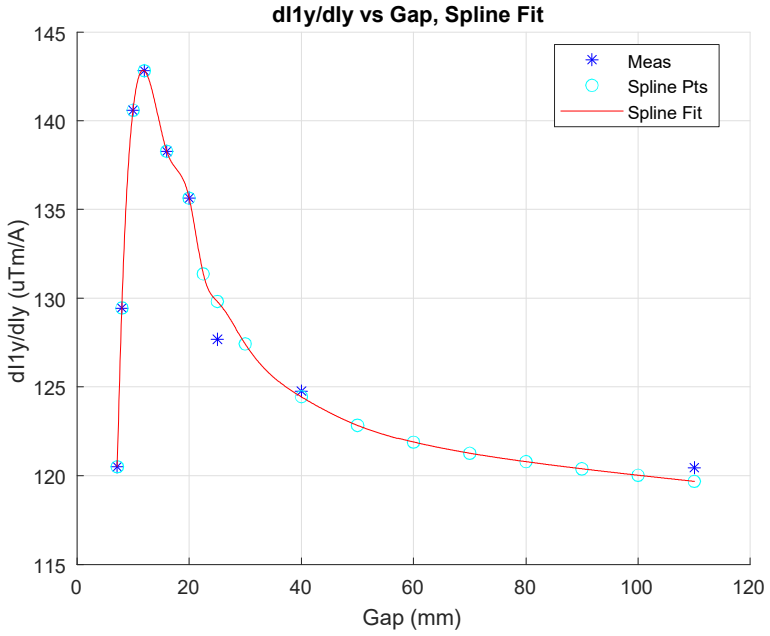

Figure 35: Response function dI_{1y}/dI_y as a function of gap for HXU-031.

7.4 Calibration

7.4.1 SXR Undulators

The external field calibration factors dI_x/dB_x and dI_y/dB_y are calculated from the results given above. They were measured on SXU-021, but we assume they are the same for all SXR undulators because of the similarity of the devices. A set of gaps are chosen and the spline fits give dI_{1x}/dB_x, dI_{1y}/dB_y, dI_{1x}/dI_x and dI_{1y}/dI_y at the chosen gaps. The ratios give the calibration factors dI_x/dB_x and dI_y/dB_y. The calibration factors as a function of gap are put into spline files. For any gap, when the calibration factor from the spline is multiplied by the difference in external field between the tunnel and the laboratory ΔB_x or ΔB_y, one gets the beam pipe corrector current required to straighten the beam trajectory.

$$I_x = \frac{dI_x}{dB_x}\Delta B_x \tag{67}$$

$$I_y = \frac{dI_y}{dB_y}\Delta B_y \tag{68}$$

The calibration factors for the SXR undulators are given in figures 36 and 37.

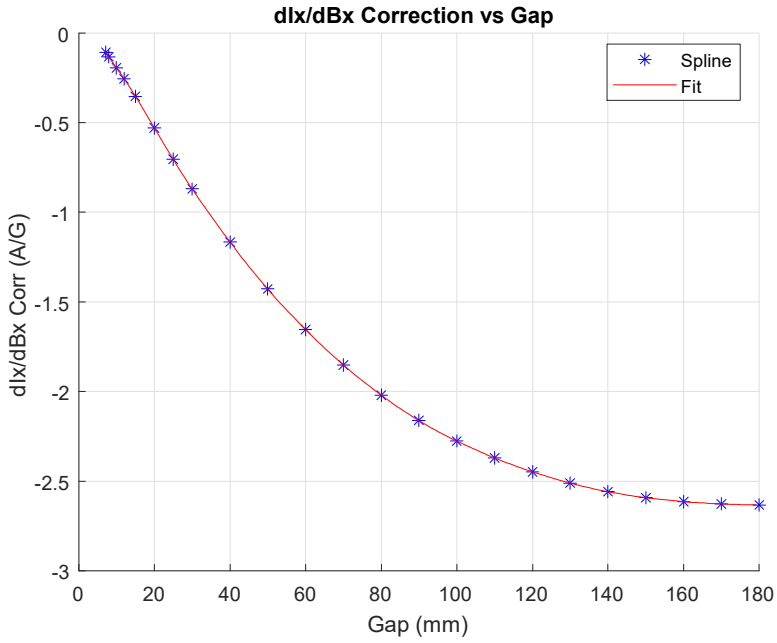

Figure 36: Calibration factor dI_x/dB_x for the SXR undulators.

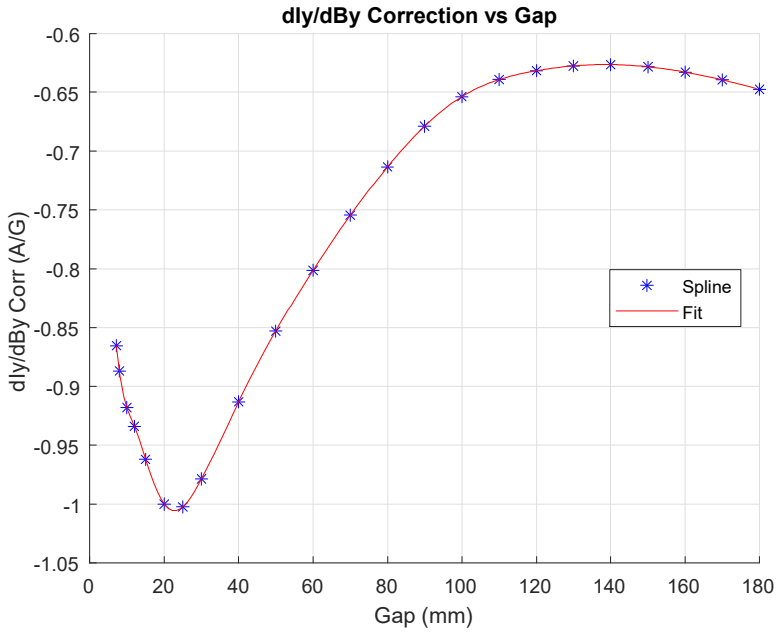

Figure 37: Calibration factor dI_y/dB_y for the SXR undulators.

7.4.2 HXR Undulators

The calibration factors for the HXR undulators are given in figures 38 and 39.

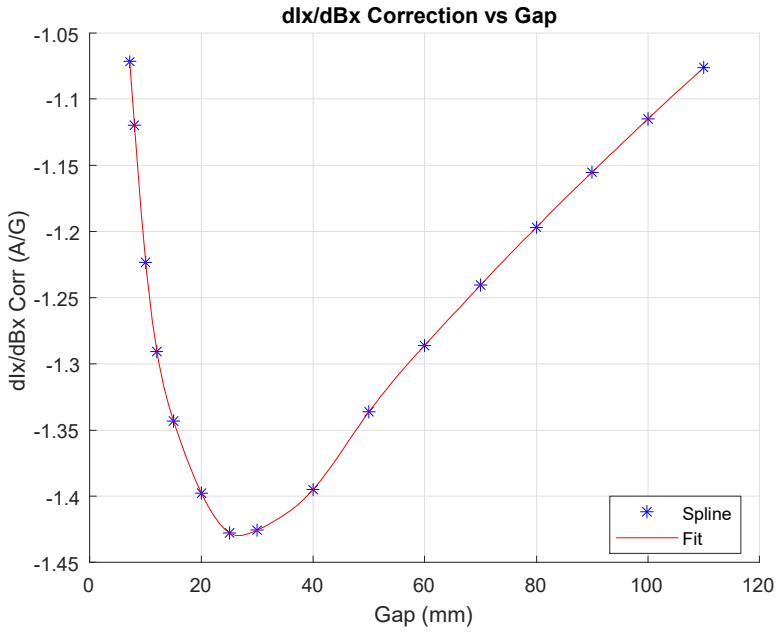

Figure 38: Calibration factor dI_x/dB_x for the HXR undulators.

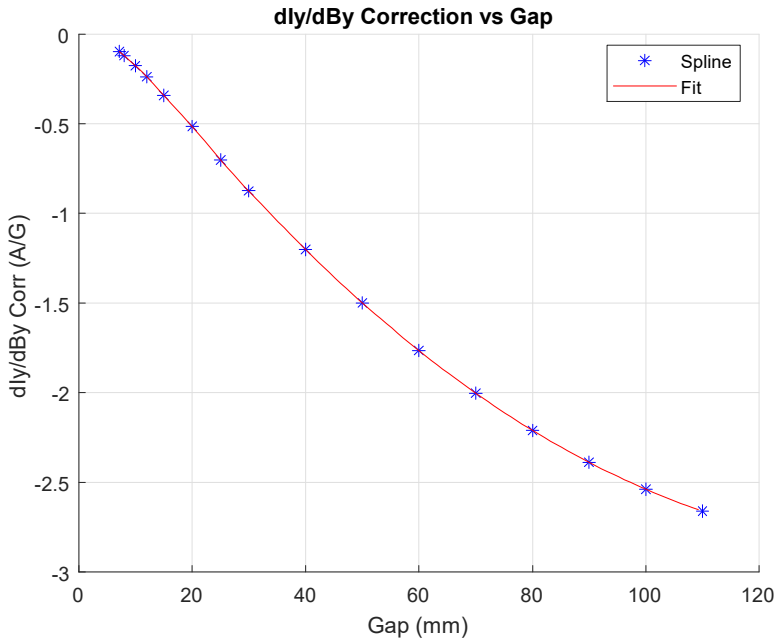

Figure 39: Calibration factor dI_y/dB_y for the HXR undulators.

8 Summary

The beam pipe corrector calibration to correct external magnetic fields was presented. For any undulator gap, a spline fit to the calibration gives a parameter dI/dB, which is multiplied by the difference in magnetic fields between the tunnel and the laboratory to give the beam pipe corrector current to correct for the field difference.

Acknowledgements

We are grateful to Heinz-Dieter Nuhn for many discussions about this work.